# A Model of the Inertial Recirculation Driven by Potential Vorticity Anomalies

PAOLA CESSI

*MIT-WHOI Joint Program in Physical Oceanography, MIT Center for Meteorology & Physical Oceanography, Cambridge, MA 02139*

GLENN IERLEY

*Department of Mathematical Sciences, Michigan Technological University, Houghton, MI 49931*

WILLIAM YOUNG

*Department of Earth, Atmospheric, and Planetary Sciences, Massachusetts Institute of Technology, Cambridge, MA 02139*

(Manuscript received 1 December 1986, in final form 23 April 1987)

ABSTRACT

Some essential features of a recirculating inertial gyre (the "recirculation") can be analyzed with a very simple, analytically tractable model. In wind-driven eddy-resolving general circulation models the recirculation appears as a strong sub-basin-scale inertial flow with homogeneous potential vorticity. The constant value of potential vorticity decreases with increasing forcing/dissipation ratio while the size and the strength of the recirculating gyre increases. In the subtropical gyre the recirculating gyre might be driven by anomalous values of low potential vorticity carried northward by the western boundary current. We have modeled this process using a barotropic model and prescribing the values of potential vorticity at the edge of the gyre. Our model gyre is contained in a rectangular box in an attempt to simplify the geometry as much as possible and to isolate the processes occurring in the recirculating region.

With weak diffusion the prescribed boundary forcing induces a flow with constant potential vorticity. We show how to calculate the homogenized value of potential vorticity in the interior without explicitly solving for the flow. We also numerically solve our model and so obtain explicit solutions. Two distinct cases arise: 1) For strong boundary forcing the gyre fills the whole box. Therefore the homogenized value of potential vorticity can be determined but the extent of the recirculation is prescribed. 2) For weak boundary forcing the recirculation fills only part of the basin and the size of the gyre must be determined as well as the homogenized value of potential vorticity within it. The latter case is the most relevant to the wind-driven, numerical experiments, because in these calculations the recirculating flow is confined to a sub-basin-scale region. Also in this case the homogenized value of potential vorticity decreases with increasing forcing, while the size and the strength of the gyre increase.

## 1. Introduction

Since Fofonoff's (1954) and Niiler's (1966) work on the free inertial circulation in a closed oceanic basin, few conceptually simple (and analytically tractable) models have been developed to understand strongly nonlinear circulation. In these early works the nonlinear, inertial gyre fills the basin. But subsequent observations, and numerical experiments, indicate that the region of strongly nonlinear, almost free, flow is confined to the northwest corner of the basin.

This "recirculation" is an oceanographically relevant phenomenon when regarding the observation of a tight subbasin-scale gyre directly south of the separated Gulf Stream. The transport of this feature is far too large to be directly driven by the observed wind system through the Sverdrup relation and indeed in eddy-resolving general circulation numerical models the westward recirculation occurs in a region pressed against the zero wind stress curl line (the northern wall in Fig. 1). It is clear that this inertial gyre is not directly wind driven but is somehow forced by the anomalous potential vorticity of the separated boundary current. It is not clear from oceanic observations whether this potential vorticity anomaly is due to buoyancy effects associated with heat loss to the atmosphere, or to northward advection of low values of planetary potential vorticity by the western boundary current.

In this article we emphasize the possible role of boundary currents as a source of low values of potential vorticity. This is principally because we compare our results with wind-driven numerical models in which this is the only process acting. However the model ultimately formulated in section 2 merely requires an external source of low potential vorticity as a driving mechanism. We do not attempt to explicitly model the processes producing the low potential vorticity.

Moore (1963) modeled the recirculation as a standing damped Rossby wave in the exit of the western boundary current. But results from general circulation

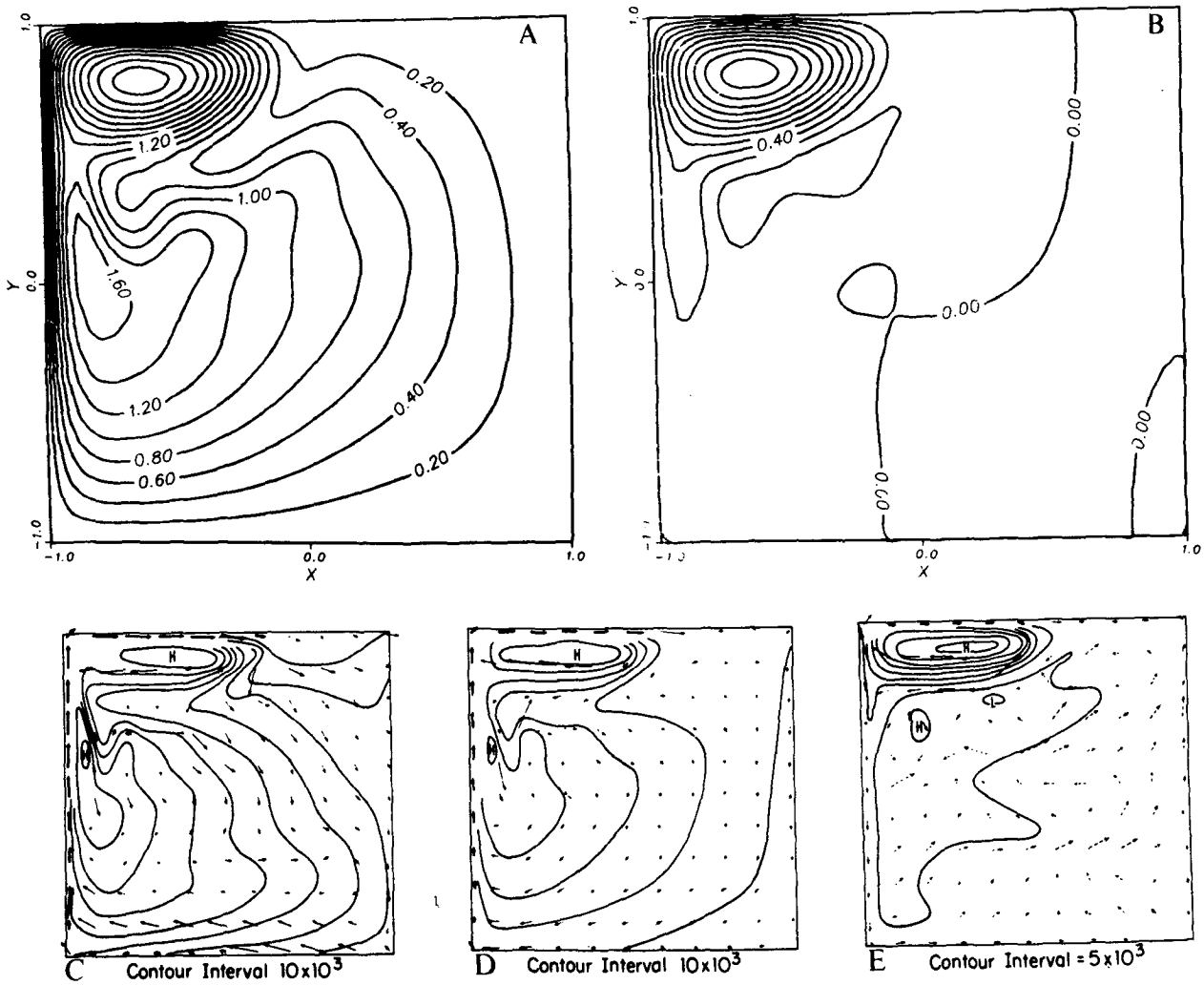


FIG. 1. Top row: steady state streamfunction resulting from a two-layer quasi-geostrophic wind-driven general circulation model. (a) Upper layer, (b) lower layer. Bottom row: Time-averaged pressure fields (solid line) and horizontal velocity (arrows) resulting from a 5-level, primitive equation, wind-driven, eddy-resolving general circulation model (Robinson et al., 1977). (c) 40 m, (d) 490 m, (e) 2690 m. These very different models produce similar large-scale circulation patterns.

models have disproved Moore's picture: both in the steady state flow (when steady equilibrium is achieved) and in the time-averaged flow (when the final equilibrium is oscillatory or chaotically eddying) the dominant feature is a "blob" of water recirculating in closed paths, rather than oscillating in a wavelike pattern. Eddy-resolving general circulation models have also clarified the role of transient small-scale features upon the mean large-scale circulation. The divergent eddy flux of vorticity points systematically down the mean potential vorticity gradient, suggesting that eddies can be parameterized as lateral diffusion of mean potential vorticity. Moreover in eddy-resolving models the recirculation zone has roughly the same horizontal extent at every depth and the strength of the flow is of the same magnitude throughout the water column. Therefore, to a first approximation the recirculation can be considered independent of depth and so a barotropic (one-layer) model may capture many of its essential features.

The purpose of this work is to isolate the main dynamical balance and driving mechanism of the recirculation using a simple, barotropic model. Before presenting this model we will summarize the results of some numerical experiments and ocean observations which motivate our formulation.

### *a. The driving mechanism*

Figure 2 shows the instantaneous streamfunction and potential vorticity fields of the final state of a general circulation model developed by one of the authors. The model is formulated using the quasi-geostrophic barotropic equation in a closed basin forced by a sim-

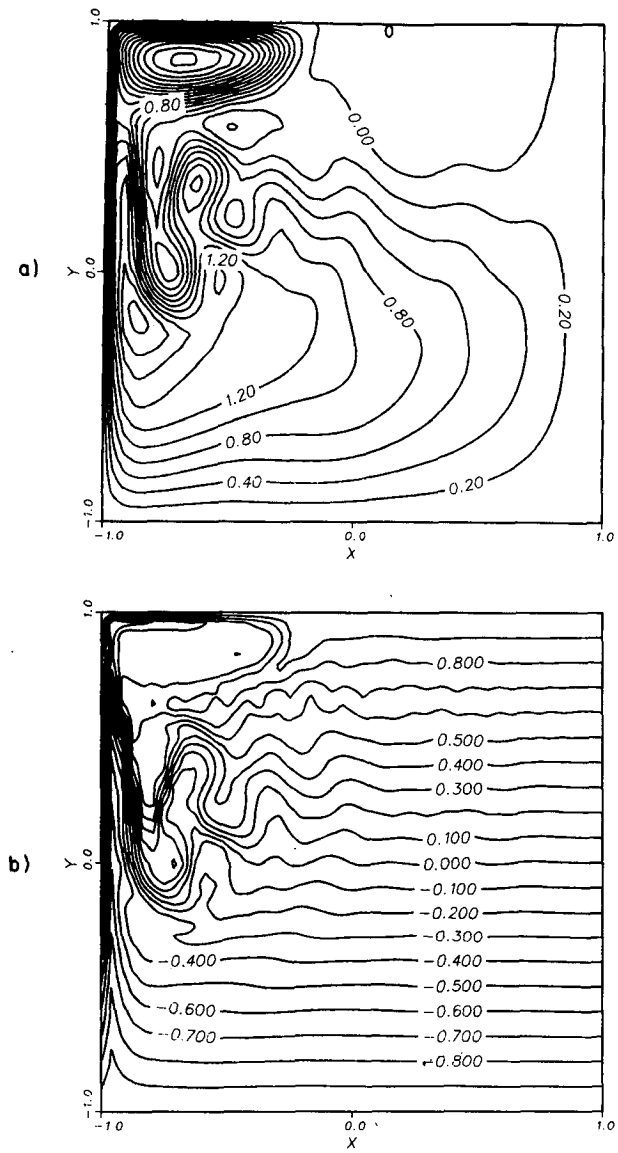


FIG. 2. Instantaneous fields at quasi-equilibrium. (a) Streamfunction, (b) potential vorticity. $y_1 = L/2$, $w_0 f_0/H\beta^2 L^2 = 10^{-3}$, $\kappa\beta H/w_0 f_0 L = 2.5 \times 10^{-2}$, $x$ and $y$ axis in units of $L$.

ple wind stress curl and damped by lateral diffusion of potential vorticity. The standard wind-driven, quasi-geostrophic formulation is

$$\frac{\partial q}{\partial t} + J(\psi, q) = f_0 w_E/H + \kappa\nabla^2 q \qquad (1.1)$$

where

$$\left.\begin{aligned} &(-\psi_y, \psi_x) = (u, v)\\ &q = \beta y + \nabla^2\psi\\ &w_E = -w_0 \cos\pi(2y + L - y_1)/2(L + y_1), \quad \text{if} \quad -L \leq y \leq y_1\\ &w_E = 0, \quad \text{if} \quad y_1 \leq y \leq L \end{aligned}\right\} \qquad (1.2)$$

with boundary conditions $\psi = \nabla^2\psi = 0$ on the boundaries $x = L, -L$; $y = L, -L$. The Ekman pumping above was first suggested by Veronis (1966) as a means of illustrating one of the essential features of recirculation, viz., it can occur entirely in a region where the wind stress curl is zero (north of $y_1$). In this experiment the western boundary current continues northward of $y_1$, turns eastward at the northern boundary, $L$, and transports low values of potential vorticity northward, where low means smaller than the local planetary vorticity. This essential feature is independent of the choice of the wind stress pattern as shown in Fig. 3, which shows the $\psi$ and $q$ time-averaged fields for the above-mentioned model, but with a wind stress curl which fills the basin, i.e., $y_1 = L$ in (1.2).

### b. *The dynamical balance*

The other feature of interest in the recirculation region is that potential vorticity is essentially homogeneous (see Figs. 2 and 3). Because the numerical model is barotropic the only term which can balance the planetary gradient, $\beta y$, is relative vorticity. Relative vorticity in these models is small in most of the basin (the external Rossby number $f_0 w_0/\beta^2 HL^2$ is $10^{-3}$), while it becomes important in the recirculation region both in the eastward and westward flow.

A very detailed diagnostic analysis of general circulation models of the type we used can be found in Böning (1986). An important conclusion of his analysis is that the dominant balance in the recirculation region is between advection of planetary vorticity and advection of relative vorticity. Dissipation becomes important only in the boundary layers around the edge of the recirculation and wind forcing is always negligible. Nevertheless dissipation is essential in determining the vorticity distribution inside the recirculation region. This is quite different from the picture envisaged by Marshall and Nurser (1986) who proposed a generalization to a baroclinic ocean of Fofonoff's (1954) calculation as a model for the inertial recirculation. In their calculations relative vorticity is neglected in the interior of the recirculation (i.e., where the flow is westward) and its effect is confined to narrow boundary layers.

The size and strength of these recirculating gyres depends sensitively on the dissipation. Figure 4 shows the solution when the diffusivity is reduced by a factor of two below that in Fig. 3. The inertial gyre is larger, its velocities are faster and the homogenized value of potential vorticity within it is reduced. This last observation is consistent with the intuitive notion that the boundary currents are more effective at transporting southern values of potential vorticity northwards when the lateral diffusivity is reduced.

One final observation from numerical experiments is that the tangent velocities at the boundary of the recirculation are essentially determined by the dynam-

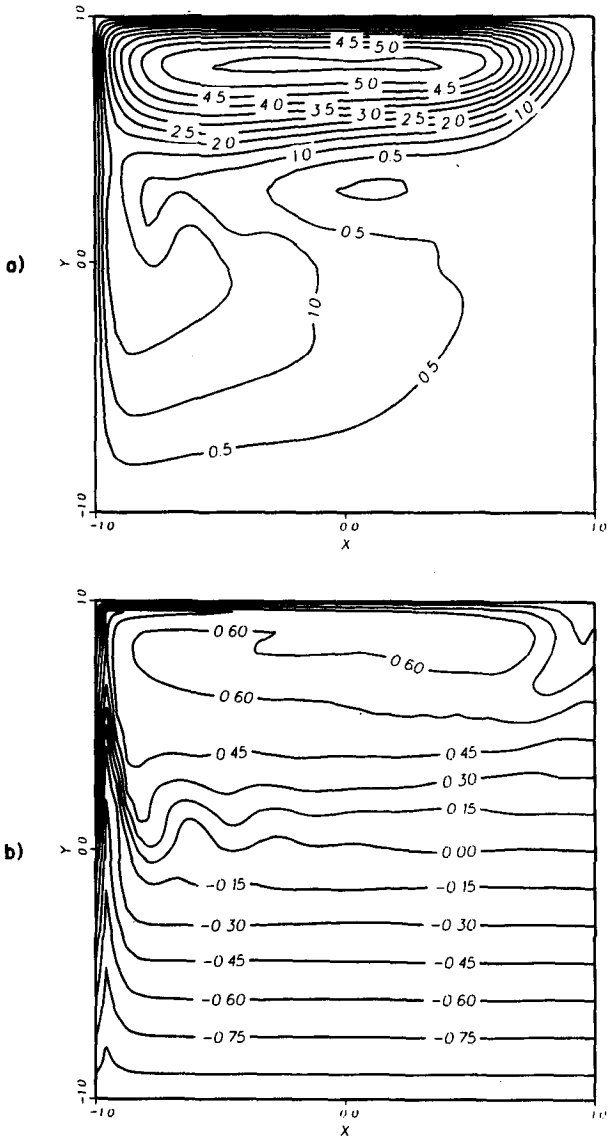


FIG. 3. Time-averaged field for the same model as in Fig. 2 except for $y_1 = L$. (a) Streamfunction, (b) potential vorticity.

ics in the interior of that region. In Fig. 5 we show the zonal velocity, $u$, and potential vorticity, $q$, in a section which cuts the recirculation region longitudinally. No jump in $u$ occurs when the northern boundary is approached. Clearly there is a jump in the shear, $\partial u/\partial y$, in order to satisfy the free slip boundary conditions, and therefore a jump in $q$, causing the second derivative of the velocity to be large near the boundary. But the essential point is that the velocity on the boundary can be predicted approximately by extrapolating its interior value from just outside the northern boundary layer.

### c. *Ocean observations*

A decisive observational test of the theory proposed here (and also that of Marshall and Nurser, 1986) would require direct measurement of relative vorticity in the westward flowing limb of the recirculation. The present model assumes that it is as large as the planetary contribution (beta times the north–south width of the recirculation) and further that both of these exceed the vortex stretching term. Unfortunately it is probably not possible to calculate the relative vorticity sufficiently accurately from observations to make this comparison.

However, one feature of the recirculation which all observers have emphasized, and which strongly supports the barotropic model used here, is the weak depth dependence of the currents in this region. Schmitz

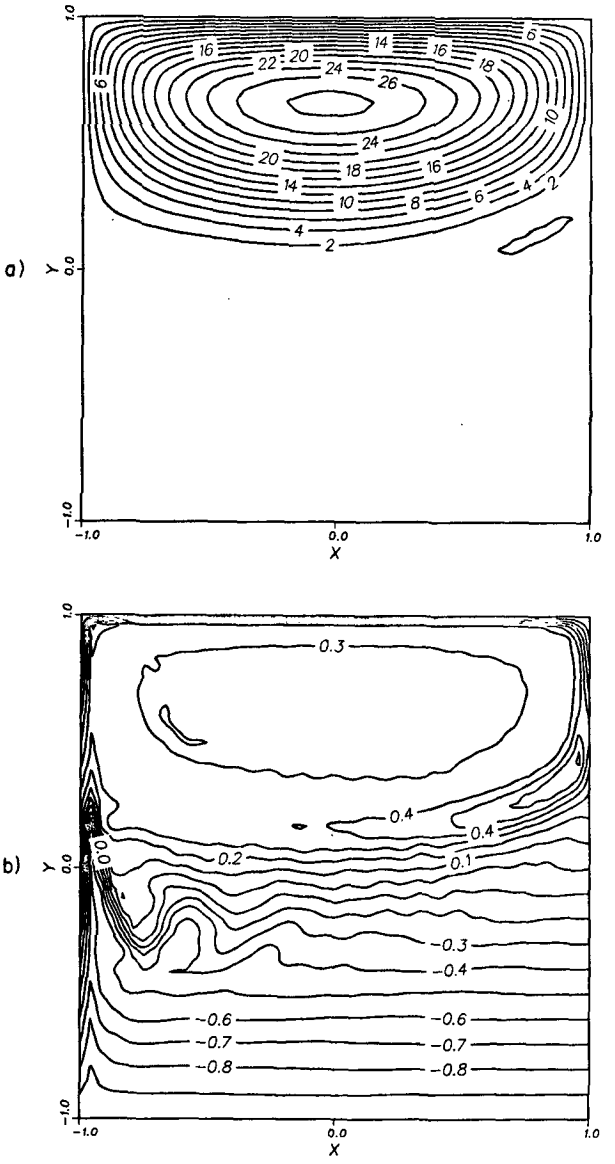


FIG. 4. As in Fig. 3 except for $\kappa\beta H/w_0 f_0 L = 1.25 \times 10^{-2}$, i.e., the diffusivity has been halved from Fig. 3. (a) Streamfunction, (b) potential vorticity.

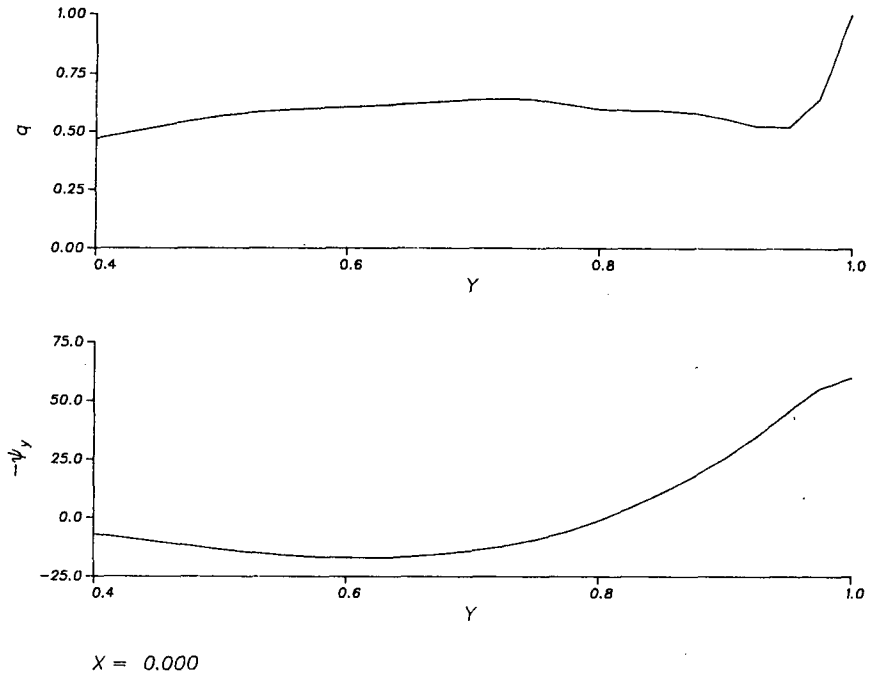


FIG. 5. (a) Zonal velocity $u$ and (b) potential vorticity $q$ through the recirculation region at $x = 0$. Notice there is no jump in velocity near the northern boundary. All parameters as in Fig. 3.

(1980) notes that in the westward recirculation the currents are both surface and bottom intensified. However the currents at middepth are certainly comparable in magnitude (10 cm $s^{-1}$) and of the same sign as the top and bottom velocities. Richardson (1985) has also emphasized the vertical coherence, down to the sea floor, of currents in the recirculation zone (see especially his Fig. 6b). Both of these studies suggest that it is the transport produced by these weakly depth-dependent currents which is responsible for the increase in Gulf Stream transport. Thus, based on these observations, the broadest conclusion one can draw is that recirculation is a barotropic phenomenon.

Of course the model formulated in section 2, which is barotropic from the outset, cannot *explain* the weak depth dependence of the recirculation. But there is a simple baroclinic extension which can be used to quantitatively assess the effects of stratification. The results of this multilayer model study, still in progress, confirm the importance of relative vorticity in the dynamic balance and also show that the recirculation will usually extend down to the sea floor.

Finally, while a detailed vorticity budget is not possible, Schmitz's current meter observations provide enough information to make an order of magnitude estimate of relative vorticity and planetary vorticity in the westward recirculation. One has

$$u_y/\beta y \sim U/\beta L^2$$

and $u = 10$ cm $s^{-1}$, $\beta = 2 \times 10^{-13}$ $cm^{-1}$ $s^{-1}$. To estimate $L$ we note that according to Schmitz the total width of the westward flowing zone is 200 km. $L$ must certainly be less than this, say 100 km, and then $U/\beta L^2 = \frac{1}{2}$, which suggests that relative vorticity is dynamically important.

### d. Summary

Recirculation is the development of a virtually barotropic, sub-basin-scale gyre in the northwest corner of the subtropical circulation. The transport of this gyre is usually observed to be larger than the Sverdrup transport by at least a factor of three. As Böning (1986) noted, the dominant balance in the barotropic potential vorticity equation is between the advection of planetary vorticity and the advection of relative vorticity. The relative vorticity is as large as the planetary vorticity even when the flow is westward. Although the dissipative terms are subdominant their strength sets the transport and size of the recirculation.

There are several questions suggested by these observations. What determines the latitudinal extent of recirculation? What determines the value of potential vorticity in the center of the homogenized gyre? It is these two related questions which the present article addresses. Additional questions such as the roles of baroclinicity, bottom drag and topography are ignored, but the model formulated in the next section can be easily extended to investigate these issues.

## 2. Formulation of the model

In order to highlight the essential features of the recirculation we will analyze a model which is as simple as possible. Specifically we will make the following assumptions:

1) The inertial recirculation is barotropic. One of the main conclusions of Böning's (1986) work is that the essential features of the recirculation found in his barotropic model are very similar to the mean transport fields of recent eddy-resolving general circulation models. Schmitz (1980) and Richardson (1985) emphasize the vertical coherence of observed currents in the Gulf Stream recirculation.

2) Relative vorticity is of the same order as planetary vorticity.

3) Diffusion is weak and can be represented as lateral diffusion of potential vorticity.

4) There is no local wind forcing. Instead the forcing is provided by prescribing the potential vorticity at the boundaries. This mimics the effect of the potential vorticity anomaly either produced by buoyancy flux or carried by the boundary current.

With the above in mind we consider the quasi-geostrophic equation in a $\beta$-plane box ($-L/\alpha < x < L/\alpha$ and $-L < y < L$)

$$\frac{\partial q}{\partial t} + J(\psi, q) = \kappa \nabla^2 q, \tag{2.1}$$

where $q = \beta y + \nabla^2\psi$ and $\alpha$ is the aspect ratio of the box. The boundary conditions are $\psi = 0$, $q = q_B(s)$ where $s$ is the arclength round the boundary. Thus, the flow is forced by the nonequilibrium distribution of potential vorticity which is prescribed at the boundary ($q_B \neq \beta y$). This forcing could be the result of diabatic effects or, as in wind-driven models, the result of a subtle balance between dissipation and advection of potential vorticity originating at lower latitudes. Because the latter process is much better documented in the literature, we will compare our results with those obtained in wind-driven ERGCMs.

The eastern and western boundaries represent the actual eastern and western boundaries of the basin, while the northern and southern boundaries are intended as the meridional boundaries of the recirculation. Implicitly we are restricting our attention to cases such as that presented in Fig. 4, where the dissipation/forcing ratio is small enough so that the recirculation region goes all the way to the eastern boundary. We discuss specific functional forms of $q_B$ in the next section.

In the steady state, some general results, which are relevant to our analysis, can be proved.

Integrating (2.1) over the area enclosed by any streamline, and assuming a steady solution, we get

$$\int \nabla q \cdot \mathbf{n} dl = 0, \tag{2.2}$$

where $\mathbf{n} = \nabla\psi/|\nabla\psi|$. That is, the total diffusive flux of vorticity across a closed streamline is zero.

Multiplying (2.1) by $\psi$ and integrating over the area enclosed by the box we obtain the energy equation

$$\frac{\partial}{\partial t}\int \frac{1}{2}(\mathbf{u})^2 dA = -\kappa \int dA(\nabla^2\psi)^2 + \kappa \int (q_B - \beta y)\mathbf{u} \cdot d\mathbf{l}. \tag{2.3}$$

This shows that in the steady state the amount of relative vorticity available in the interior is proportional to the relative vorticity circulated at the boundaries. If, as a trivial example, $q_B = \beta y$, then the relative vorticity must be identically zero everywhere in the interior and therefore there is no flow. This emphasizes the role of $q_B$ as forcing.

Equation (2.1) is analogous to an advection–diffusion equation for the concentration of a passive tracer with prescribed values at the boundaries. It is intuitively clear that the concentration in the interior must have values lying between the boundary values. That is, the maximum and minimum values of $q$ are on the boundary. Nevertheless, since potential vorticity is not a passive tracer, we will prove this result rigorously. The following never uses the connection between $\psi$ and $q$ and so applies equally well to a passive scalar.

Suppose there is a point in the interior where $q$ is larger (smaller) than any of the values of the boundaries. If this occurs, such a point is a maximum (minimum). Therefore, around this point there will be a nested set of closed $q$ contours. Integrating (2.1) over the area enclosed by any such contour we get

$$0 = \int \nabla^2 q dA = \oint \nabla q \cdot \mathbf{n} dl = \int |\nabla q| dl, \tag{2.4}$$

which is a contradiction. Hence, there are no closed $q$ contours and no extrema in the interior. From this "extremum principle" we infer that there are no shear layers[1] in the domain. In such a layer $\nabla^2\psi$ must become very large so that the potential vorticity in the layer would exceed the boundary values.

Notice that in deriving these general results we have not made any assumption about the size of dissipation. In order to make further progress we will examine the limit in which diffusion is weak, a limit which is probably the most relevant for the oceanic recirculation.

## 3. Homogenized gyre filling the domain

In the steady state (2.1) can be written as

$$J(\psi, q) - \kappa \nabla^2 q = 0.$$

With simple choices of $q_B$, we have solved the above equation numerically using Newton's method, which

[1] A shear layer is an internal boundary layer where a discontinuity in velocity is smoothed over a distance which decreases as the diffusivity, $\kappa$, is reduced.

is much more efficient than time integration. Specifically we have chosen

$$q_B = (Q_n - Q_s)(y - L)/2L + Q_n, \tag{3.1}$$

where $Q_n$ and $Q_s$ are the (constant) values of $q$ on the northern and southern boundaries, respectively. The specification of $q_B$ above is the simplest possible and it is hoped to investigate other more realistic choices at a later date. Typical steady state solutions are shown in Figs. 6, 7 and 8. For some choices of $Q_n$ and $Q_s$ the recirculating gyre fills the whole box, while for other choices it is confined to part of the basin. In this section we will analyze cases where the circulation fills the whole domain as in Fig. 6. The more complicated and interesting case typified by Fig. 8 will be analyzed in section 4.

In the limit of weak diffusion, outside the thin boundary layers which are close to the solid walls, the potential vorticity is homogeneous (Fig. 6). This is a consequence of (2.2) in the limit of small dissipation (see Rhines and Young, 1982, for a detailed discussion). But what is the constant value of potential vorticity inside the recirculation region?

This question is answered in appendix A and the conclusion is that the constant value of potential vorticity in the interior is given by

$$\bar{q} = \oint q_B \mathbf{u} \cdot d\mathbf{l} \Big/ \oint \mathbf{u} \cdot d\mathbf{l}, \tag{3.2}$$

where both integrals are performed along the boundary of the domain. A detailed derivation is given in appendix A, but the physical explanation of this remarkable result is simple. As the fluid is advected along the streamlines, potential vorticity is diffused from streamline to streamline. Streamwise diffusion is always negligible with respect to advection and cross-stream diffusion. On the other hand, cross-stream diffusion is more effective where streamlines are closer together, i.e., where the velocities are larger (Roberts, 1977; Young, 1984). This is why, in the determination of $\bar{q}$, the boundary values of $q$ contribute more where the velocities are *larger*. Notice that this "velocity weighted" average is quite opposite to a time average which would be weighted with the inverse of the velocity. Thus, perhaps counterintuitively, the places where the fluid spends the most time contribute least to the value of $\bar{q}$.

As was noted at the end of the introduction, and illustrated for the wind-driven case in Fig. 5, the velocity at the boundary is essentially determined by the interior dynamics where potential vorticity is constant. In the present model this is guaranteed by the extremum principle which excludes shear layers. In the interior region the potential vorticity is uniform and the flow satisfies

$$\nabla^2 \psi + \beta y = \bar{q}, \tag{3.3}$$

with boundary conditions $\psi = 0$ on $x = \pm L/\alpha$ and $y$

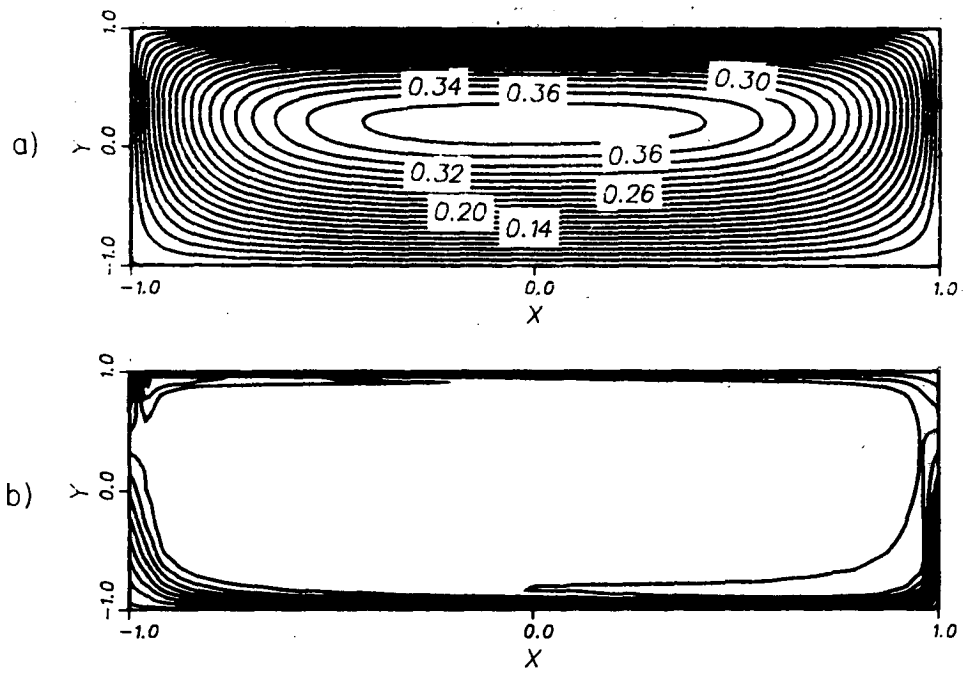


FIG. 6. (a) Streamfunction and (b) potential vorticity for the steady state resulting from the numerical solution of (2.1). $Q_n = -2\beta L/3$, $Q_s = -\beta L$, $L = 300$ km, $\beta = 2 \times 10^{-13}$ cm$^{-1}$ s$^{-1}$, $\alpha = 0.3$, $\kappa = 2.43 \times 10^6$ cm$^2$ s$^{-1}$. Streamfunction is in units of $\beta L^3 = 5.4 \times 10^5$ m$^2$ s$^{-1}$, $x$ axis in units of $L/\alpha$, $y$ axis in units of $L$. Potential vorticity contour interval is 0.03. Notice the presence of small closed $q$ contours, due to small residual time dependence.

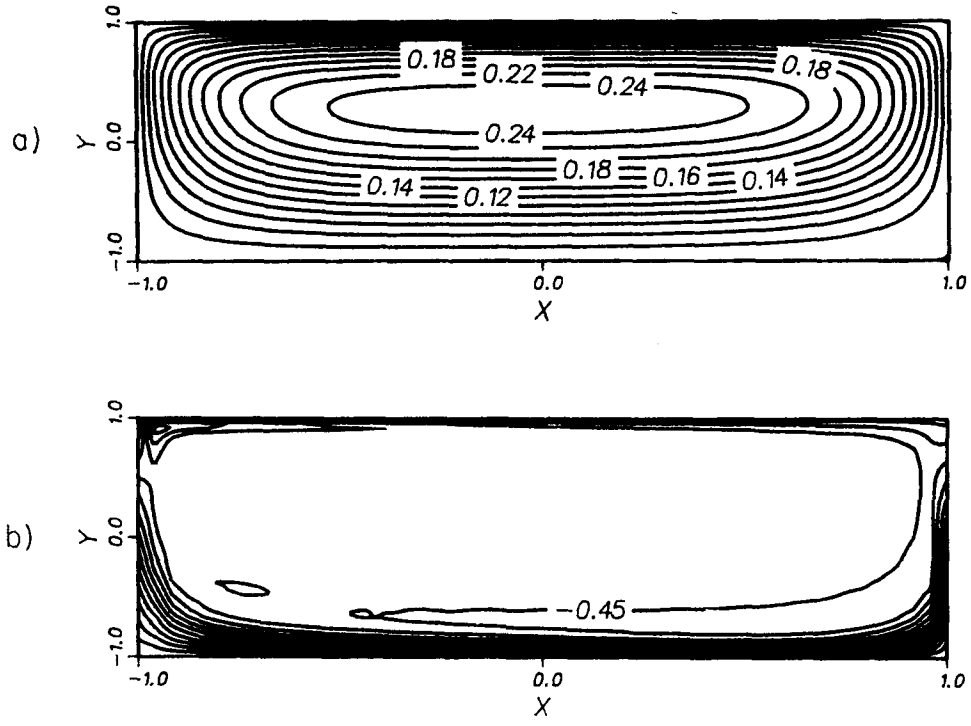


FIG. 7. (a) Streamfunction and (b) potential vorticity for the steady state resulting from the numerical solution of (2.1). $Q_n = -\beta L/3$, $Q_s = -\beta L$, $L = 300$ km, $\beta = 2 \times 10^{-13}$ cm$^{-1}$ sec$^{-1}$, $\alpha = 0.3$, $\kappa = 2.43 \times 10^6$ cm$^2$ s$^{-1}$. Streamfunction is in units of $\beta L^3 = 5.4 \times 10^5$ m$^2$ s$^{-1}$. $x$ axis in units of $L/\alpha$, $y$ axis in units of $L$. Potential vorticity contour interval is 0.05.

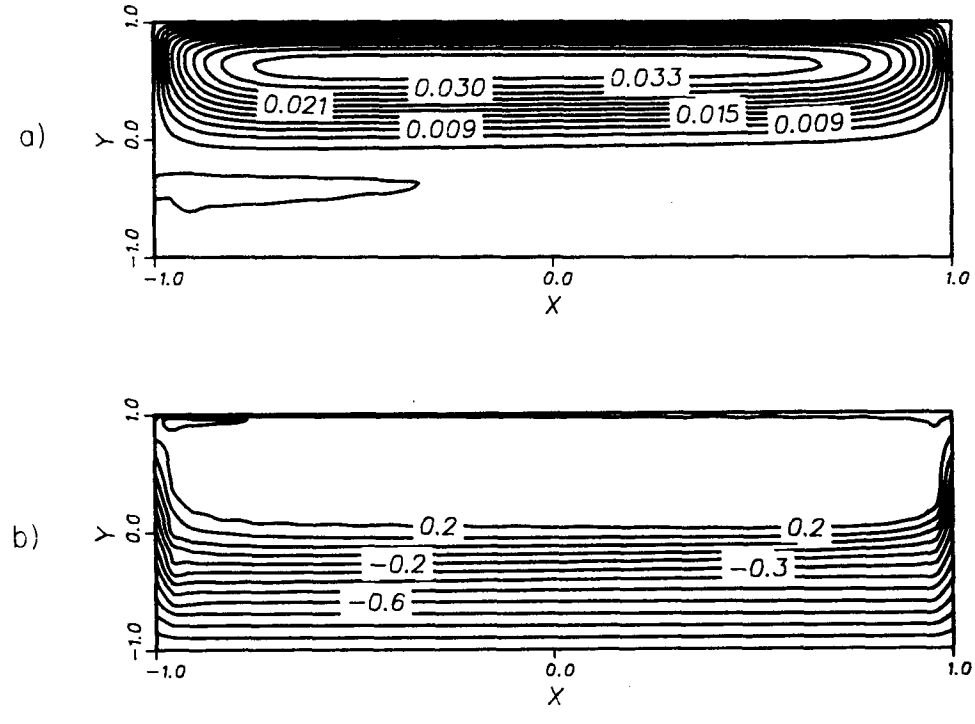


FIG. 8. (a) Streamfunction and (b) potential vorticity for the steady state resulting from the numerical solution of (2.1). $Q_n = \beta L/3$, $Q_s = -\beta L$, $L = 300$ km, $\beta = 2 \times 10^{-13}$ cm$^{-1}$ s$^{-1}$, $\alpha = 0.3$, $\kappa = 8.1 \times 10^5$ cm$^2$ s$^{-1}$. Streamfunction is in units of $\beta L^3 = 5.4 \times 10^5$ m$^2$ s$^{-1}$. $x$ axis in units of $L/\alpha$, $y$ axis in units of $L$.

$= \pm L$. Using this result and the choice (3.1), the expression (3.2) for $\bar{q}$ can be put in the form

$$\bar{q} = \int dA q_B(\bar{q} - \beta y) \Big/ \int dA(\bar{q} - \beta y). \qquad (3.4)$$

This result can be generalized for any choice of $q_B$ at the boundary as shown in appendix B. Evaluating the trivial integrals above yields a simple quadratic equation for $\bar{q}$ with solutions:

$$\bar{q} = (Q_n + Q_s)/4 \pm [(Q_n + Q_s)^2/16 - \beta L(Q_n - Q_s)/6]^{1/2}. \qquad (3.5)$$

In deriving (3.5) we have implicitly assumed that the solution of (3.3) and (3.5)

(i) fills the whole domain and
(ii) has only one gyre.

Both of these assumptions must be checked a posteriori by solving (3.3) and (3.5). In this way certain unphysical roots are eliminated. This task is simplified by noting that (3.5) gives real solutions only for certain choices of $Q_n$, $Q_s$ and $L$. Actually (3.5) depends only on the two nondimensional parameters $n = Q_n/\beta L$ and $s = Q_s/\beta L$, and in Fig. 9 the parabola bounding the domain of real solutions in the $(n, s)$ plane is shown. Notice the symmetry around the axis $n = -s$. Changing $n + s$ into $-(n + s)$ keeping $n - s$ constant just reverses the sign of $\bar{q}$. Therefore we only need to analyze the half-plane $n + s \leqslant 0$. It should be noted that (3.5) is independent of the longitudinal scale of the basin, $\alpha$. This is due to the choice for the boundary value of $q$ in (3.1) which does not depend on longitude.

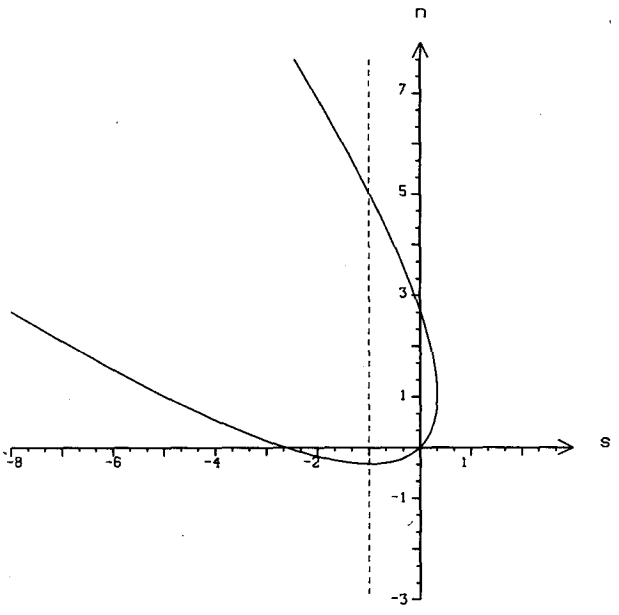


FIG. 9. Parabola bounding the domain of real solutions to (3.5) as a function of $n = Q_n/\beta L$ and $s = Q_s/\beta L$. Inside the parabola (3.5) has complex roots. The dashed line is at $s = -1$.

As we mentioned earlier, the homogenized value of $q$ in the interior of the basin, given by (3.5), must be consistent with the assumptions made to derive this result. Specifically it must be such that the solution of (3.2) consists of only one gyre which fills the box. Whether this is the case or not depends on $\bar{q}$ and on the geometry of the basin, i.e., $\alpha$. Therefore the choice of a specific geometry restricts the allowable values of $\bar{q}$ and the values of $n$ and $s$ for which there is one gyre which fills the domain. In other words, deciding which solutions of (3.4) are physical is straightforward but tedious. There is a three-dimensional parameter space: $n$, $s$, and $\alpha$. Even after eliminating obviously spurious solutions, such as complex values of $\bar{q}$, or values which lie outside the interval $(Q_s, Q_n)$, the task is beyond the scope of this paper and probably not very rewarding. Instead, using physical arguments, we now restrict attention to a certain portion of parameter space ($s = -1$, $n < 1$, $\alpha \ll 1$) which is particularly relevant to the wind-driven models, which initially motivated (2.1).

In the wind-driven models the main source of vorticity for the recirculation is the western boundary current. As the flow rushes along the streamlines surrounding the recirculation it carries low values of potential vorticity while dissipation acts to bring potential vorticity back to its local planetary value. Therefore, at the northern boundary the potential vorticity has a value lower than the local planetary vorticity ($n < 1$). At the southern boundary the recirculation is bounded by the Sverdrup interior where relative vorticity is negligible. Therefore we have concentrated our attention on cases where the southern edge of the box containing the recirculation is a "shearfree" latitude, i.e., $Q_s = -\beta L$. In Fig. 9 this corresponds to the line $s = -1$. Figure 10 is a summary of (3.5) for the choice $s = -1$, as a function of $n$. For $n < -\frac{1}{3}$ only one solution is physically acceptable, for $-\frac{1}{3} < n < 5$ both solutions are complex and finally for $n > 5$ both solutions are physically acceptable.

For example, at the point $s = -1$, $n = -\frac{2}{3}$, (3.5) gives two roots: $\bar{q} = -0.76\beta L$ and $\bar{q} = -0.073\beta L$. The latter is clearly unphysical because it gives a value for the homogenized $q$, which is outside the boundary values. Figure 6 shows the numerical steady state solution found by Newton's method. In this run $Q_n = -2\beta L/3$ and $Q_s = -\beta L$. The agreement with the theoretical prediction is very good. In this case the gyre fills the whole basin and the homogenized value for $q$ is between $-0.73\beta L$ and $-0.76\beta L$.

## 4. Homogenized gyre with free boundary

The case which is most relevant to the wind-driven experiments is when the forcing provided by the potential vorticity boundary condition is weak. That is, when the values of $Q_n$ and $Q_s$ are chosen such that (3.5) does not have real roots. A trivial example of weak forcing is the point $n = 1$, $s = -1$ in Fig. 9, which

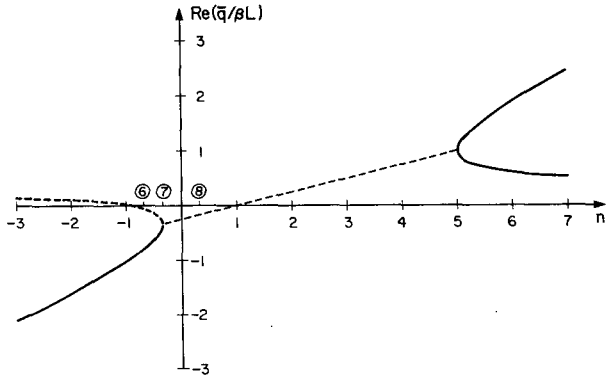


FIG. 10. The real part of $\bar{q}$ as a function of $n$ calculated from (3.5) setting $s = -1$. The dashed curve represents unphysical solutions ($\bar{q}$ complex or $\bar{q}$ outside the range of boundary values). The parameter setting used in Figs. 6, 7 and 8 are indicated by the numbers in circles.

would correspond to the choice $q_B = \beta y$ for the boundary value of potential vorticity. Clearly no gyre can develop for this choice because no forcing is applied at the boundary.

We have run our numerical model choosing $Q_n = \beta L/3$ and $Q_s = -\beta L$. This corresponds to the point $n = 1/3$ and $s = -1$ in Fig. 9. In Fig. 8 we show the $\psi$ and $q$ fields resulting from our numerical run. There is a narrow gyre pressed against the northern wall and a very weak, $O(\kappa)$, flow filling the rest of the box. Although we try to impose the scale of the gyre by specifying the box, the circulation picks its own boundary and fills only part of the domain. The situation is illustrated schematically in Fig. 11: the recirculation fills only the portion of the basin from $y_s$ to $L$ and south of $y_s$ essentially no circulation occurs. Now the southern edge of the recirculation is not a solid wall but a free streamline and this imposes some constraints on the flow. Specifically the tangential velocity has to be constant on a free streamline $y_s$, and in this particular problem the constant is zero. If it were not zero, velocity would be discontinuous at $y_s$ inducing large shears that would violate the extremum principle.

Notice that because the tangential velocity is zero at

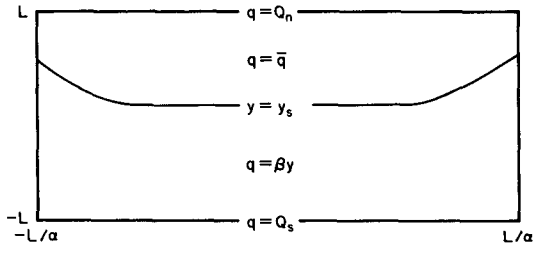


FIG. 11. Schematic picture of Fig. 8, showing the flow regimes in different regions. South of the free streamline $y = y_s(x)$ the fluid is at rest. North of $y_s(x)$ the fluid circulates with uniform potential vorticity. At the free streamline, $y_s(x)$, both $\psi$ and $\nabla\psi$ are zero.

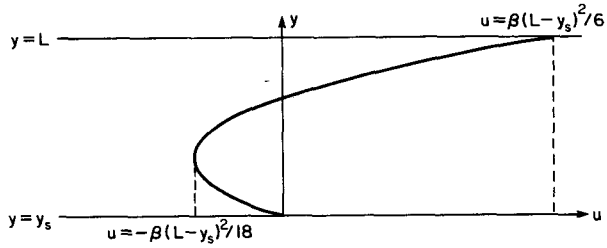


FIG. 12. Zonal velocity profile resulting from (4.3a). The minimum velocity occurs at $y - y_s = (L - y_s)/3$ and the velocity vanishes at $y - y_s = 2(L - y_s)/2$.

the southern edge of the recirculation, the unknown boundary value of $q$ at that location does not affect the "velocity weighted" average (3.2). Therefore the homogenized value of $\bar{q}$ will be close to the northern boundary value $Q_n$, and indeed in Fig. 8, where $Q_n/\beta L = 1/3$ and $Q_s/\beta L = -1$, the homogenized value of potential vorticity inside the gyre is $q/\beta L \approx 0.3$.

The condition that the southern edge of the recirculation, $y_s$, is a free streamline ($\psi = 0$ and $\nabla\psi = 0$) sets a relation between the homogenized value of $\bar{q}$ and the meridional scale of the gyre. Equation (3.2) gives a second relation between $y_s$ and $\bar{q}$. These two relations determine completely the problem of finding $y_s$ and $q$ once the boundary value for $q$ is specified on the western, northern, and eastern walls.

The solution of (3.3) in the case where the southern boundary is an unknown streamline at which both $\psi$ and $\nabla\psi$ vanish is a very hard problem in an arbitrary geometry. In the following we will obtain a simple approximate solution for gyres where the meridional scale is much smaller than the longitudinal scale ($\alpha \ll 1$). In this small aspect ratio limit, and away from the eastern and western walls, the problem is approximately one dimensional. Thus (3.3) becomes

$$\psi_{yy} + \beta y = \bar{q}, \tag{4.1}$$

with boundary conditions $\psi = 0$ on $y = L$, $y_s$ and additionally

$$\psi_y = 0 \quad \text{on} \quad y = y_s. \tag{4.2}$$

Thus, we are imposing three boundary conditions on the second-order problem (4.1). The problem has a solution because $y_s$ is also an unknown.

The solution of (4.1) which satisfies the boundary conditions is

$$\psi = -\beta(y - L)(y - y_s)^2/6$$
$$\bar{q} = \beta(L + 2y_s)/3. \tag{4.3}$$

In the approximation $\alpha \ll 1$ the "average" value of potential vorticity inside the gyre is simply given by

$$\bar{q} = Q_n,$$

and (4.3b) can be written as

$$(L - y_s) = 3(\beta L - Q_n)/2\beta. \tag{4.4}$$

This shows that the width of the gyre is proportional to the forcing, $\beta L - Q_n$, applied at the northern wall, and is independent of the size of the box.

For the simple solution (4.3) the maximum transport is given by

$$\psi_{\max} = (\beta L - Q_n)^3/12\beta^2. \tag{4.5}$$

Notice that $\beta L - Q_n$ can be eliminated between (4.4) and (4.5) so that the maximum transport is proportional to the cube of the meridional extent of the gyre. This result completes the analogy with the wind-driven experiments. As the forcing increases (lower values of $q$ are introduced at the northern boundary) the recirculation gyre expands, the homogenized value of potential vorticity decreases and the strength of the circulation increases. Figure 12 shows the parabolic, zonal velocity profile calculated from (4.3a). Note that the region of westward flow is twice as wide as the region of eastward flow. Further the maximum eastward velocity is three times as large as the maximum westward velocity. Let us now compare our theoretical prediction for the homogenized value of potential vorticity $\bar{q}$ and the meridional scale of the gyre (4.4) with the numerical results shown in Figs. 7 and 8.

For the run shown in Fig. 7, $Q_n = -\beta L/3$, $Q_s = -\beta L$: our result (4.4) gives $\bar{q} = -\beta L/3$ and $y_s = -L$, i.e., the recirculating gyre just fills the whole basin and the southern solid boundary is a free streamline. The result from the numerical experiment is $\bar{q} = -4.6\beta L$ and $y_s \approx -L$.

For the run shown in Fig. 8, $Qn = \beta L/3$, our prediction (4.4) gives $\bar{q} = \beta L/3$ and $y_s = 0$, i.e., the recirculation fills half of the basin, while the numerical experiment gives $\bar{q} = 0.3\beta L$ and $y_s \approx 0$. Both experiments are in excellent agreement with the theoretical prediction.

## 5. Conclusions

We have analyzed a simple analytical model which highlights some essential features of the subbasin recirculating gyre appearing in many eddy-resolving numerical models of the wind-driven general circulation. The characteristics of the recirculation in these numerical models are: (i) the recirculation is barotropic to a first approximation; (ii) relative vorticity is as important as planetary vorticity even where the flow is westward; (iii) the recirculation is driven by anomalous values of potential vorticity carried northward (in the subtropical gyre) by the western boundary current; and (iv) the transport exceeds the Sverdrup transport by at least a factor of three.

In formulating our model we have assumed that the recirculation is inertial and barotropic and we have simplified the driving mechanism by prescribing anomalous values of potential vorticity at the edge of the inertial gyre. Also we have isolated our model gyre from the Sverdrup interior by enclosing it in a box of simple rectangular geometry and ignoring the Ekman pumping and any diabatic effects. Even after these simplifications the problem is nonlinear because relative vorticity is essential. Some progress can be made analytically in the limit of weak diffusion. In this limit the prescribed boundary forcing induces a flow in the interior whose potential vorticity is uniform. Because there is no vortex stretching this implies that relative vorticity balances planetary vorticity in such a way as to keep total potential vorticity constant. Thus the relative vorticity is dynamically essential even where the flow is westward.

We have calculated the homogenized value of $q$ without first solving for the explicit solution. In particular, we have shown that the homogenized value in the interior is given by the averaged boundary values of $q$ weighted by the boundary values of the velocity.

In the case of weak boundary forcing the gyre is confined to a sub-basin region. This case is the most relevant to the wind-driven experiments. For weak forcing we can calculate the size of the recirculation region as well as the homogenized value of $q$.

In the wind-driven experiments the homogenized value of potential vorticity decreases as the forcing gets stronger or the dissipation weakens, while the size and strength of the recirculation increase, e.g., Figs. 3 and 4. This is exactly what happens in our model gyre: as the northern boundary value is lowered below the local planetary value the meridional scale of the gyre increases. Specifically, (4.4) shows that the size of the gyre is linearly proportional to the relative vorticity at the northern boundary. At the same time (4.5) shows that the strength of the gyre increases as the cube of the width. For a gyre 450 km wide and 2700 m deep, our model predicts a maximum transport of 121.5 Sv ($\text{Sv} \equiv 10^6\ \text{m}^3\ \text{s}^{-1}$), which is in good agreement with the results of the numerical model of Robinson et al. (1977).

In all the cases presented in this work a very simple form of boundary forcing in (3.1) has been used. Specifically the boundary condition for $q$ is constant along the northern boundary of the basin. Therefore our recirculating gyre occupies the whole basin in the longitudinal direction. On the other hand, the boundary forcing along the eastern and western boundaries decreases with decreasing latitude and sometimes the gyre occupies only part of the basin in the meridional direction. Additional numerical experiments, which will be reported in a separate paper, show that if the forcing on the northern boundary is also decreasing in the positive $x$-direction then the gyre is confined to the northwestern corner of the basin. This is consistent with the observation that in the wind-driven experiment, for moderate values of diffusion, the gyre is separated from the eastern boundary as in Figs. 1 and 2 (remember that the forcing in these experiments is provided by the western boundary current).

The "$q$-driven" model we have presented here can be extended in a number of directions. For example

different, and perhaps more realistic, boundary distributions can be used to force the flow. The effects of baroclinicity can be assessed in a straightforward way by adding layers. Bottom drag and topography are easily included. The question that one is avoiding is how to relate $q_B(s)$ to the boundary layer dynamics or diabatic processes, which one supposes are responsible for the anomalous potential vorticity at the rim of the circulation. This is an important open question that the preceding discussion has ignored. But this is also a strength of the $q$-driven model. It enables one to decrease the diffusivity while holding the boundary forcing fixed. This is not possible in the wind-driven models where a reduction in dissipation simultaneously changes *both* the boundary layer potential vorticity transport and the inertial recirculation produced by it. In this wind-driven case it is therefore impossible to perform a controlled experiment in which structure of the nonlinear, sub-basin-scale mode is cleanly revealed.

*Acknowledgments.* WRY was supported by NSF 8421074-OCE, GRI by NSF 8415702-OCE and PC by NSF ATM84-13515. We thank Dorothy Frank and Charmaine King for their assistance with the preparation of this manuscript. Computational resources were generously provided by the Michigan Technological University Academic Computer Service.

## APPENDIX A

### Derivation of the "Velocity Weighted" Average, (3.2)

The result (3.2) holds if instead of potential vorticity we consider the more general problem of a generic passive tracer which satisfies the advection diffusion equation

$$J(\psi,\theta)=\kappa\nabla^2\theta$$

$$\psi=0,\quad \theta=\theta_B \text{ on the boundary.} \tag{A1}$$

Multiplying by $\psi$ and integrating over the area of the box we eventually obtain

$$\int dA\theta\nabla^2\psi=\oint\theta_B\mathbf{u}_B\cdot d\mathbf{l}. \tag{A2}$$

In the limit of small diffusion, $\theta$ will be given by its homogenized value $\bar{\theta}$ everywhere except in narrow boundary layers close to the edge of the gyre. Therefore, in this strongly advective limit the left-hand side of (A2) can be approximated.

$$\int dA\theta\nabla^2\psi\approx\bar{\theta}\int dA\nabla^2\psi, \tag{A3}$$

and (A2) becomes

$$\bar{\theta}=\frac{\oint\theta_B\mathbf{u}_B\cdot d\mathbf{l}}{\oint\mathbf{u}_B\cdot d\mathbf{l}}. \tag{A4}$$

This result is implicit in Roberts' (1977) work. His derivation made use of local coordinates to express the dominant balance in (A1), while we prefer the integral balance (A4) because it provides an explicit formula for the interior homogenized value of the tracer concentration. The velocity weighted average (A4) is confirmed by the numerical experiment of Musgrave (1985). In his work he showed that a passive tracer satisfying (A1), in the presence of a western intensified flow, would homogenize in the interior to the value on the western boundary. Interestingly enough, the derivation that leads to (A4) can be used for potential vorticity, which is not a passive tracer. Because of the extremum principle the relative vorticity is bounded by its boundary values and so is finite everywhere in the domain, including the boundary layers. Therefore the approximation (A3) holds for potential vorticity as well as for a passive tracer. Moreover the velocity at the boundary, $\mathbf{u}_B$, can be approximated with the interior velocity just outside the boundary layer, and this allows the complete determination of the homogenized value of potential vorticity without a detailed boundary layer solution.

## APPENDIX B

### How to Find $\bar{q}$ without Solving for the Flow

The velocity weighted average (3.2) can be written as

$$\bar{q}=\frac{\oint q_B(\nabla\psi)\cdot\mathbf{n}dl}{\oint\nabla\psi\cdot\mathbf{n}dl}.$$

Since $q_B$ is only defined on the boundary we have the freedom of defining a function $g$ everywhere in the domain such that

$$\nabla^2 g=0 \text{ in the interior and}$$

$$g=q_B \text{ on the boundary.} \tag{B1}$$

With this choice and using Gauss' theorem, $\oint q_B\times(\nabla\psi)\cdot\mathbf{n}dl$ becomes $\int dAg\nabla^2\psi$ and the expression for the averaged $q$ is

$$\bar{q}=\frac{\int dAg(\bar{q}-\beta y)}{\int dA(\bar{q}-\beta y)},$$

where $g$ is a known function, independent of $\psi$, which satisfies (B1).

## REFERENCES

Böning, C. W., 1986: On the influence of frictional parameterization on wind-driven ocean circulation models. *Dyn. Atmos. Oceans*, **10**, 63–92.

Fofonoff, N. P., 1954: Steady flow in a frictionless homogeneous ocean. *J. Mar. Res.*, **13,** 254–262.

Marshall, J. C., and G. Nurser, 1986: Steady, free circulation in a stratified quasi-geostrophic ocean. *J. Phys. Oceanogr.*, **16,** 1799–1813.

Moore, D. W., 1963: Rossby waves in ocean circulation. *Deep-Sea Res.*, **10,** 735–748.

Musgrave, D. L., 1985: A numerical study of the roles of subgyre-scale mixing and the western boundary current on homogenization of a passive tracer. *J. Geophys. Res.*, **90,** 7037–7043.

Niiler, P. P., 1966: On the theory of wind-driven ocean circulation. *Deep-Sea Res.*, **13,** 597–606.

Rhines, P. B., and W. R. Young, 1982: Homogenization of potential vorticity in planetary gyres. *J. Fluid Mech.*, **122,** 347–367.

Richardson, P. L., 1985: Average velocity and transport of the Gulf Stream near 55°W. *J. Mar. Res.*, **43,** 83–111.

Roberts, G. O., 1977: Fast viscous convection. *Geophys. Astrophys. Fluid Dyn.*, **8,** 197–233.

Robinson, A. R., D. E. Harrison, Y. Mintz and A. J. Semtner, 1977: Eddies and the general circulation of an idealized oceanic gyre: A wind and thermally driven primitive equation numerical experiment. *J. Phys. Oceanogr.*, **7,** 182–207.

Schmitz, W. J., 1980: Weakly depth-dependent segments of the North Atlantic circulation. *J. Mar. Res.*, **38,** 111–133.

Veronis, G., 1966: Wind-driven ocean circulation. Part II: Numerical solutions of the nonlinear problem. *Deep-Sea Res.*, **13,** 31–55.

Young, W. R., 1984: The role of western boundary layers in gyre-scale ocean mixing. *J. Phys. Oceanogr.*, **14,** 478–483.